Supporting Information for *Acta Phys. -Chim. Sin.* doi: 10.3866/PKU.WHXB201909035

用于长期神经电生理记录的自伸展电极阵列

王璐璐[1,2,†]，谢泽鑫[1,†]，钟成[1]，唐永强[1,2]，叶丰明[1,2]，王立平[1,*]，鲁艺[1,*]

[1] 中国科学院深圳先进技术研究院，脑认知与脑疾病研究所，深港脑科学创新研究院，广东 深圳 518055

[2] 中国科学院大学，深圳先进技术学院，广东 深圳 518055

Self-spreadable Octopus-like Electrode Arrays for Long-term Neural Recordings

Lulu Wang [1,2,†], Zexin Xie [1,†], Cheng Zhong [1], Yongqiang Tang [1,2], Fengming Ye [1,2], Liping Wang [1,*], Yi Lu [1,*]

[1] The Brain Cognition and Brain Disease Institute, Shenzhen Institutes of Advanced Technology, Chinese Academy of Sciences; Shenzhen-Hong Kong Institute of Brain Science-Shenzhen Fundamental Research Institutions, Shenzhen 518055, Guangdong Province, P. R. China.

[2] Shenzhen College of Advanced Technology, University of Chinese Academy of Sciences, Shenzhen 518055, Guangdong Province, P. R. China.

[*]Corresponding authors. Emails: luyi@siat.ac.cn (Y.L.); lp.wang@siat.ac.cn (L.W.). Tel.: +86-755-86132705 (Y.L.); +86-755-86910600 (L.W.).

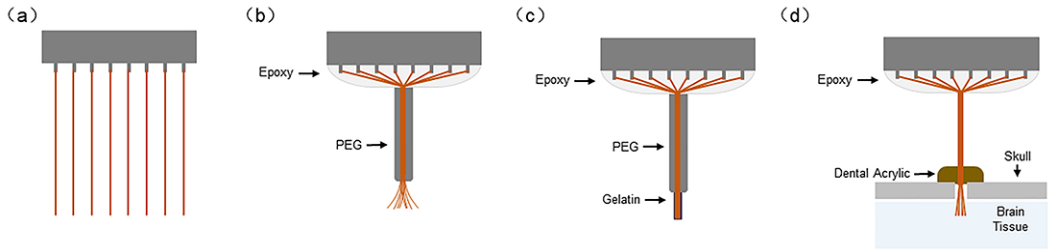

Fig. S1 The fabrication and implantation procedure of octrode array.

Recording channels (microwires) were gathered together (a) and enwrapped with PEG (b). (c) The tip of electrode array was gathered together using a thin gelatin layer. (d) After implantation, the gelatin was quickly dissolved and the recording channels were self-spread *in vivo* due to the pre-stress of the gathered microwires.

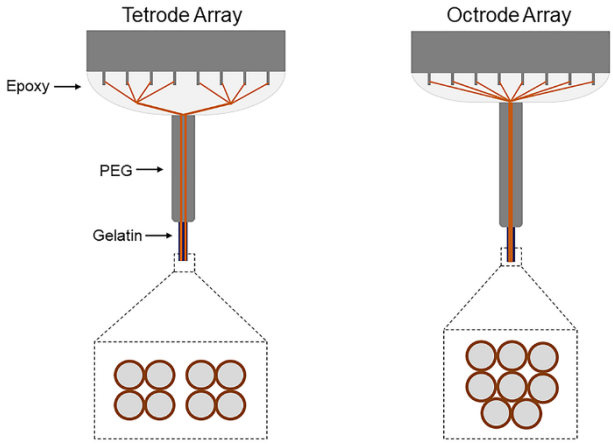

Fig. S2 The diagrams of the fabricated tetrode and octrode array.

To systematically investigate the characteristics of self-spreadable electrodes in vivo, we compared the performance of 8-channel electrode (octrode) arrays with 8-channel tetrode (bi-tetrode) arrays. As the cross-section area of each electrode array was determined by the number of recording channels (microwires), therefore, the estimated insertion trauma of the octrode array was similar to that of the tetrode array.

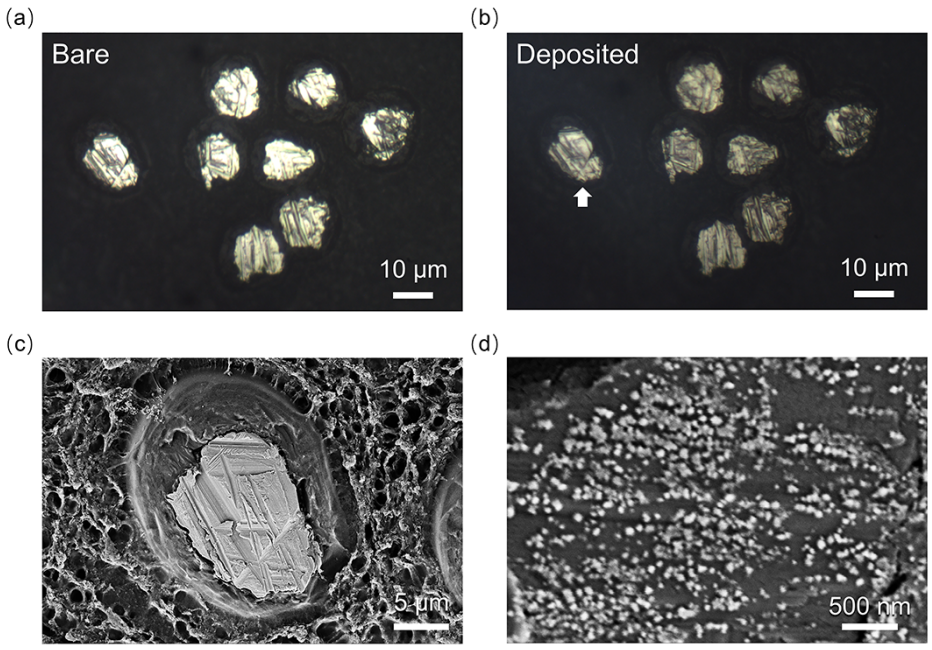

Fig. S3 Surfaces of octrode arrays.

Optical images of octrode array before (a) and after (b) Pt deposition. Under metallographic microscope, the untreated octrode array showed a light-yellow metallic color, while the surface of Pt deposited octrode array was grey-yellow. (c–d) SEM images of Pt deposited octrode surface (enlargement of arrow-pointed area in figure b). The surface of Pt deposited octrode array exhibited numerous tiny particles in the nanometer scale ranging from 20 to 50 nm. This structure significantly enlarged the electro-active area at the electrode/tissue interface and may consequently reduce its impedance.

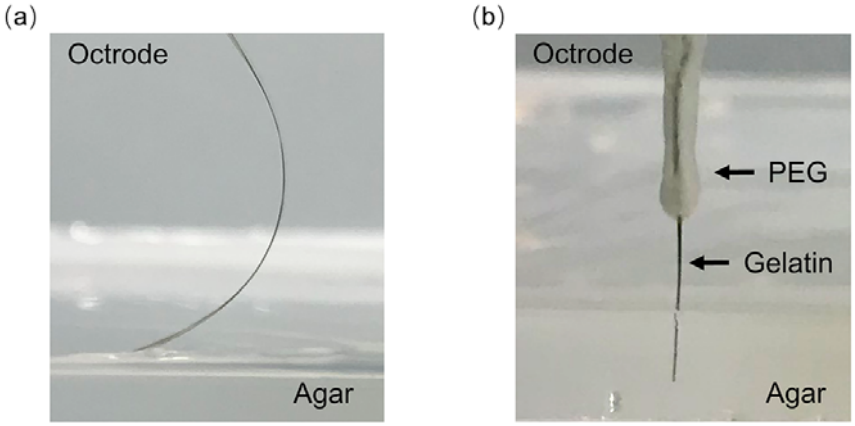

Fig. S4 Enwrapped PEG supporting layers and gelatin coating significantly enhanced the mechanical strength of octrode array for implantation.

(a) Uncoated octrode array. (b) PEG supporting layers and gelatin coated octrode array. As the octrode array was too soft to be inserted into the agar phantom, we enwrapped the octrode array with PEG supporting layers and gelatin coating. This dual coating strategy significantly enhanced the mechanical strength of octrode array during implantation without causing additional insertion trauma.

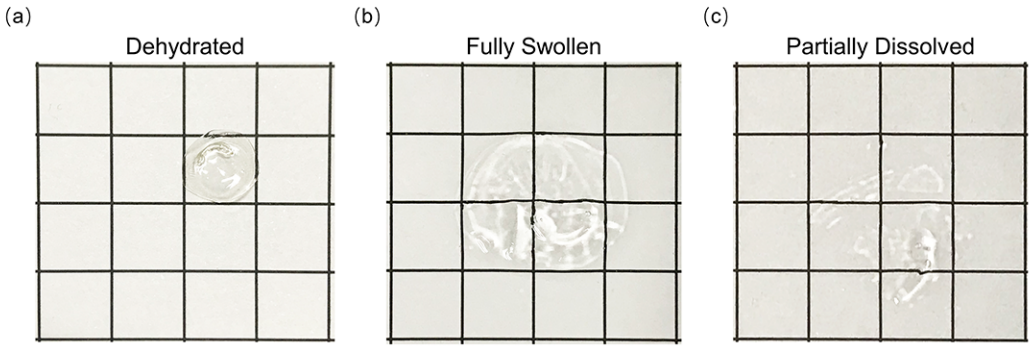

Fig. S5 Images of dehydrated (a), fully swollen (b) and partially dissolved (c) gelatin samples.

The dehydrated gelatin thin film (diameter = 10 mm, thickness = 0.3 mm) swelled quickly (linear expansion ratio > 100%) and then dissolved in ACSF.

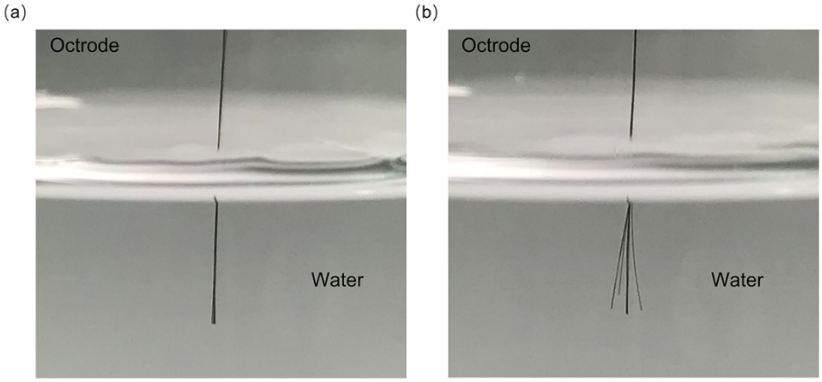

Fig. S6 The self-spreading process of octrode array.

(a) The dehydrated gelatin coating is stiff enough to maintain the architecture of octrode array.

(b) The tip of octrode array was self-spread within 20 minutes after being inserted into water.

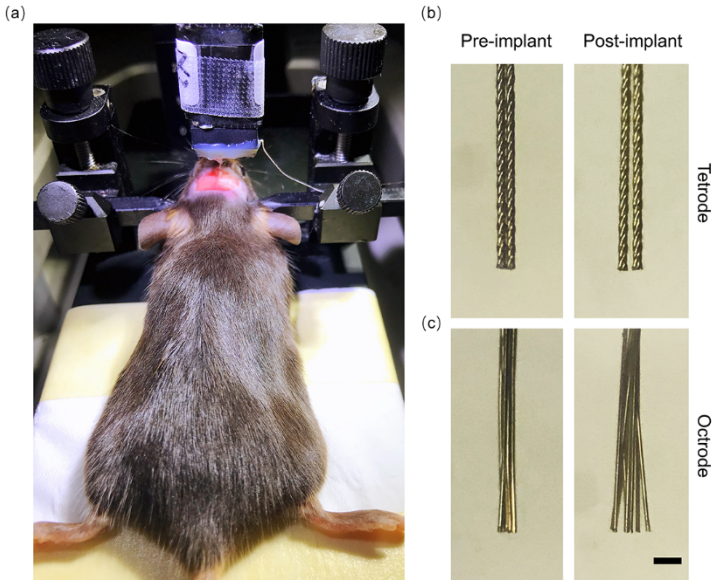

Fig. S7 Implantation of electrode arrays.

(a) A representative image of implantation procedure. Representative images of tetrode (b) and octrode (c) arrays before and after implantation. Scale bar, 100 μm.

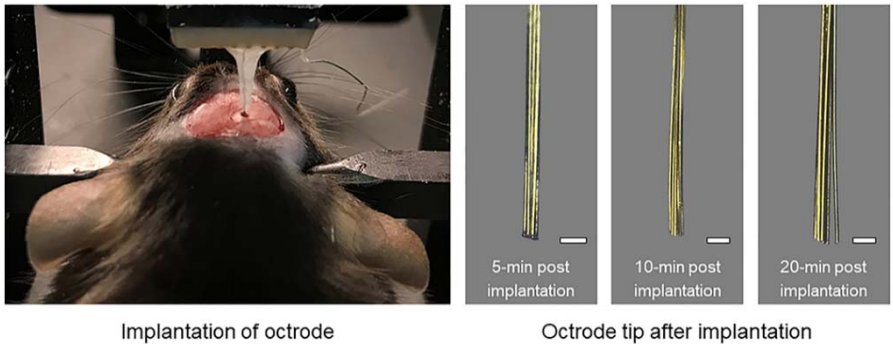

Fig. S8 The swelling and dissolution process of gelatin coating and the self-spreading of octrode array.

The tip of electrode was coated with an ultra-thin layer of gelatin to enhance its mechanical strength for implantation. To investigate the swelling and dissolution process of the gelatin coating and assess the acute damage of octrode to the brain tissue, gelatin coated octrodes were inserted into the hippocampus of C57 mice and then were gently raised out of the brain at different time points. No significant change of the octrode was observed after a 5-min acute implantation, and the electrode diameter was approximately 70 μm. At 10 mins post implantation, the octrode tip was partially self-spread. At 20 mins post implantation, the octrode tip was fully self-spread, implying a dissolution of the gelatin coating. These results suggest a quick swelling and dissolution process of the gelatin coating, which did not significantly increase the octrode size and cause additional insertion trauma during implantation. Scale bar, 100 μm.

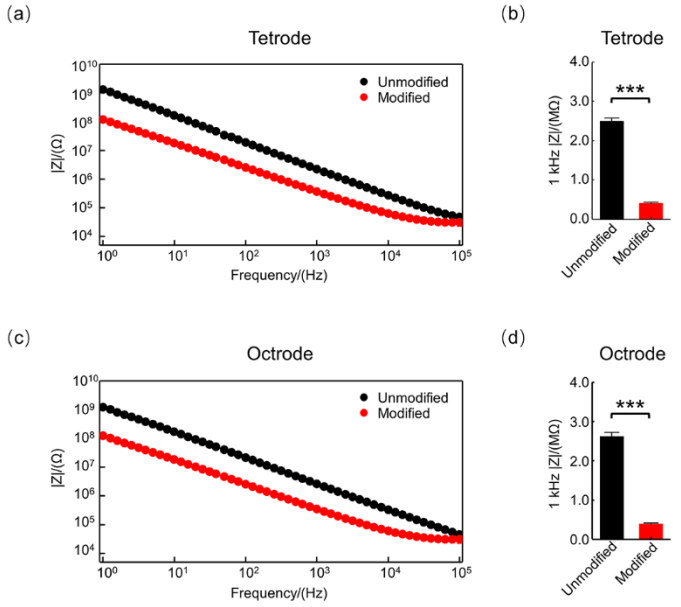

Fig. S9 EIS analysis before and after Pt deposition.

(a, c) The EIS of tetrode (a) and octrode (c) arrays before and after modification. (b, d) Impedance (at 1 kHz) of tetrode (b) and octrode (d) arrays. Data are presented as mean ± standard error of the mean; $n = 8$ in each group; ***, $p<0.005$. EIS tests were performed on the first recording channel (Ch01) of each electrode array. The average impedance (at 1kHz) of tetrodes before and after Pt deposition were 2.49 ± 0.08 MΩ and 0.41 ± 0.02 MΩ, respectively. The average impedance (at 1kHz) of octrodes before and after Pt deposition were 2.63 ± 0.10 MΩ and 0.39 ± 0.02 MΩ, respectively.

Table S1 Fitting data for proposed equivalent circuit model shown in Fig. 1.

Parameters	**Units**	**Tetrodes (n = 9)**	**Octrodes (n = 9)**
Z **(at 1 kHz)**	**MΩ**	1.50 ± 0.05	1.26 ± 0.08
R_T	**kΩ**	61.10 ± 2.17	61.57 ± 1.94
CPET-q	**nFs^{n-1}**	1.56 ± 0.44	7.21 ± 5.00
CPET-n	**$0 \leq n \leq 1$**	0.77 ± 0.03	0.73 ± 0.03
CPED-q	***nFs^{n-1}***	1.70 ± 0.61	3.14 ± 0.62
CPED-n	**$0 \leq n \leq 1$**	0.52 ± 0.12	0.47 ± 0.11
R_D	**MΩ**	1.67 ± 0.56	1.21 ± 0.21
T_D	**ms**	0.72 ± 0.19	0.69 ± 0.17

The equivalent circuit model for the implanted electrode interface comprises these circuit elements: tissue resistance (R_T), electrode-tissue constant-phase element (ZCPE-T), double-layer constant-phase element (ZCPE-D), and finite-length Warburgh diffusion impedance (Z_D). The constant-phase element (CPE) represents a dispersive double-layer capacitance, which reflects the non-homogeneity of the microscopic distribution at the electrode/polymer/neural-tissue interface. The CPE concept is described using this equation:

$$\mathrm{ZCPE} = 1/\{q(j\omega)n\}, \qquad (1)$$

where $j = \sqrt{-1}$, ω is the angular frequency (rad/s) = 2πf, and f is the frequency in Hz. The CPE is defined by two parameters, q and n. Parameter q indicates the value of the capacitance of the CPE as n approaches 1, and has a numerical value of 1/ZCPE at ω = 1 rad/s. Parameter n reveals the micro fractal and distribution at the electrode/tissue interface, and it correlates to a series of factors such as charge-transfer rates or distributions. When n = 1, the CPE is identical to a capacitor.

The finite-length Warburg diffusion impedance (Z_D) is used to describe ion diffusion at the electrode/tissue interface. Z_D is described by the following equation:

$$Z_D = R_D \coth\{(j\omega T_D)1/2\}/(j\omega T_D)1/2, \qquad (2)$$

where R_D is the diffusional resistance and T_D is the diffusional time constant.

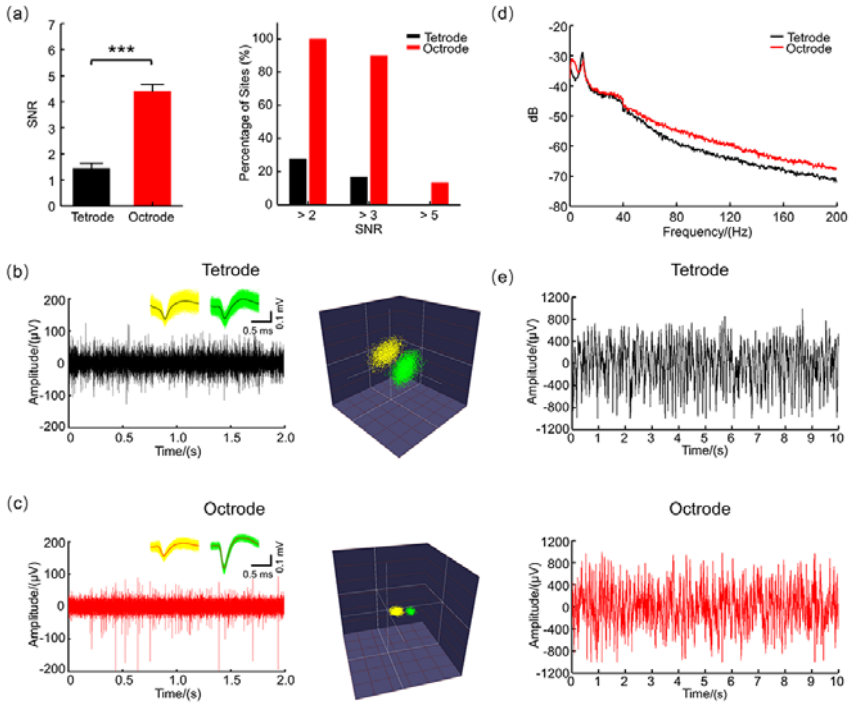

Fig. S10 Electrophysiological characterizations on day 7 post-implantation.

(a) Signal-to-noise ratio (SNR) of recorded hippocampal neurons using tetrode (n = 6 mice) and octrode (n = 5 mice) arrays (mean ± standard error of the mean), and percentage of medium (SNR > 2), high (SNR > 3) and extra high (SNR > 5) quality units. The average SNR of tetrode and octrode arrays were 1.44 ± 0.20 and 4.41 ± 0.26, respectively. The percentages of recorded waveforms which were categorized as medium-SNR and high-SNR waveforms in the cases of tetrode arrays were only 27.8% and 16.7% respectively, while the respective percentages for the octrode arrays were 100% and 90%. Furthermore, none of the waveforms recorded by tetrode arrays were categorized as extra high-SNR waveforms, compared to 13.3% for the octrode arrays. (b–c) Representative examples of raw spike traces, principal-component analysis (PCA) and waveforms of neuronal units recorded by a tetrode (b) and a channel of an octrode array (c), respectively. Low-amplitude spikes are not shown in PCA. Different types of neural waveforms can be clearly isolated by both tetrode and octrode arrays. (d) Average power spectra of LFPs recorded by tetrode (n = 6 mice) and octrode (n = 5 mice) arrays. (e) Representative examples of raw LFPs recorded by tetrode and octrode arrays.

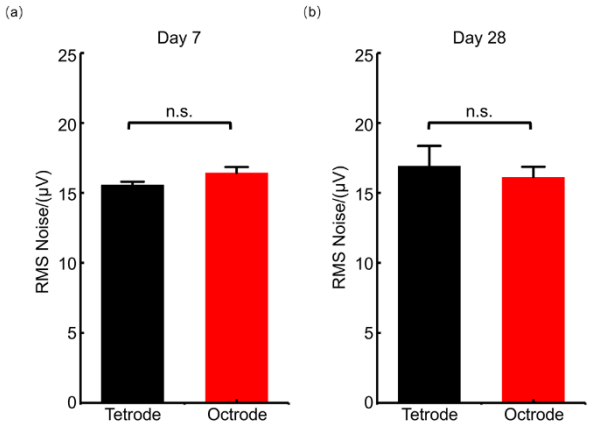

Fig. S11 Average RMS noise of tetrode and octrode arrays on day 7 (a) and day 28 (b) after implantation.

On day 7, the average RMS potentials of the tetrodes and octrodes were 15.58 ± 0.23 μV (mean ± standard error of the mean, n = 6 mice) and 16.43 ± 0.43 μV (mean ± standard error of the mean, n = 5 mice), respectively. On day 28, the average RMS potentials of the tetrodes and octrodes were 16.92 ± 1.44 μV (mean ± standard error of the mean, n = 6 mice) and 16.13 ± 0.74 μV (mean ± standard error of the mean, n = 5 mice), respectively. No significant differences were observed between the tetrodes and octrodes.

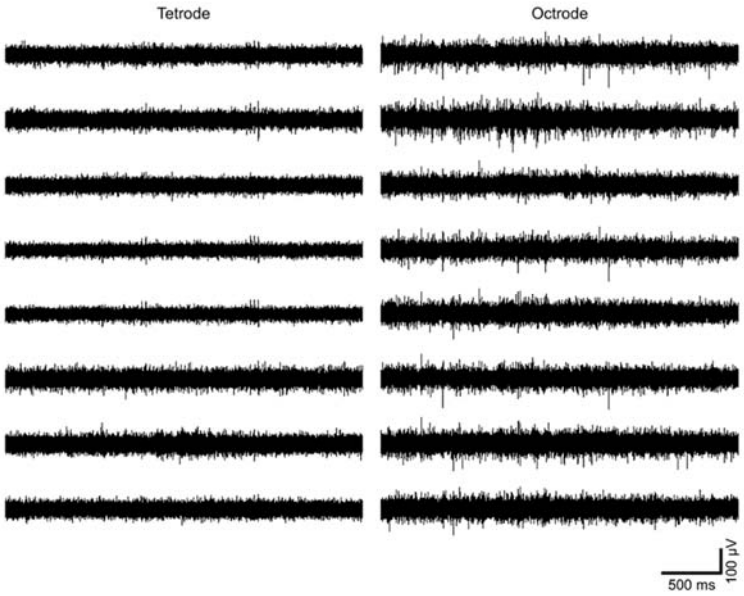

Fig. S12 Representative example of raw spike recordings in hippocampus using tetrode (left) and octrode (right) arrays on day 28.

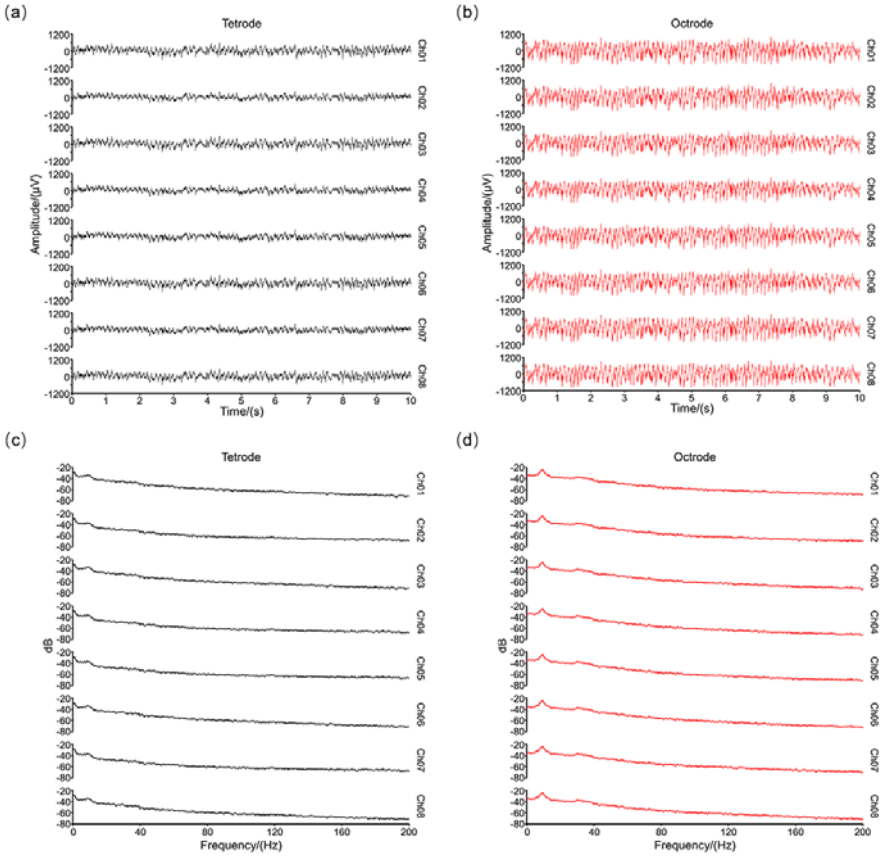

Fig. S13 Representative example of raw LFPs (a, b) and power spectra of LFPs (c, d) recorded by tetrode and octrode arrays.

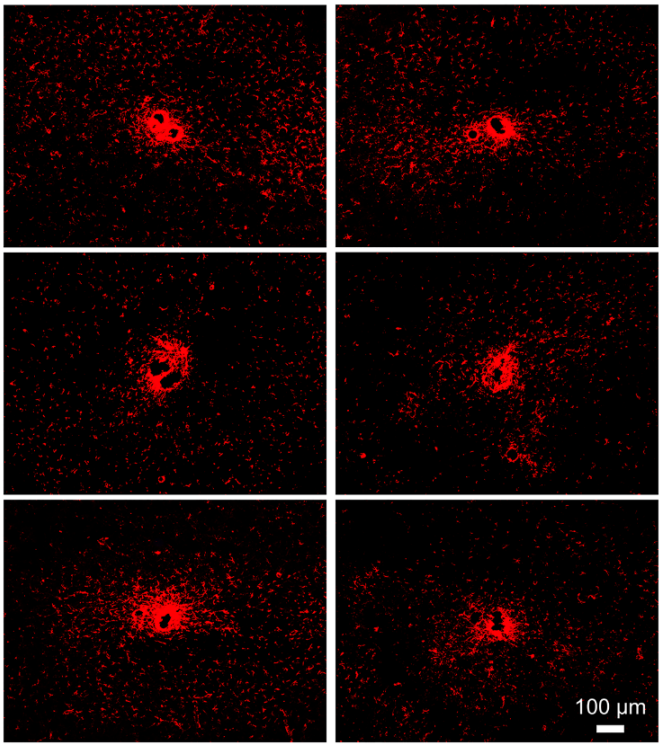

Fig. S14 GFAP immunostaining of tetrode arrays after 4 weeks post-implantation.

Representative images were obtained from the subjects in the tetrode group (subject number: tetrode02-07), respectively. Representative image of subject "tetrode01" is shown in Fig. 3a.

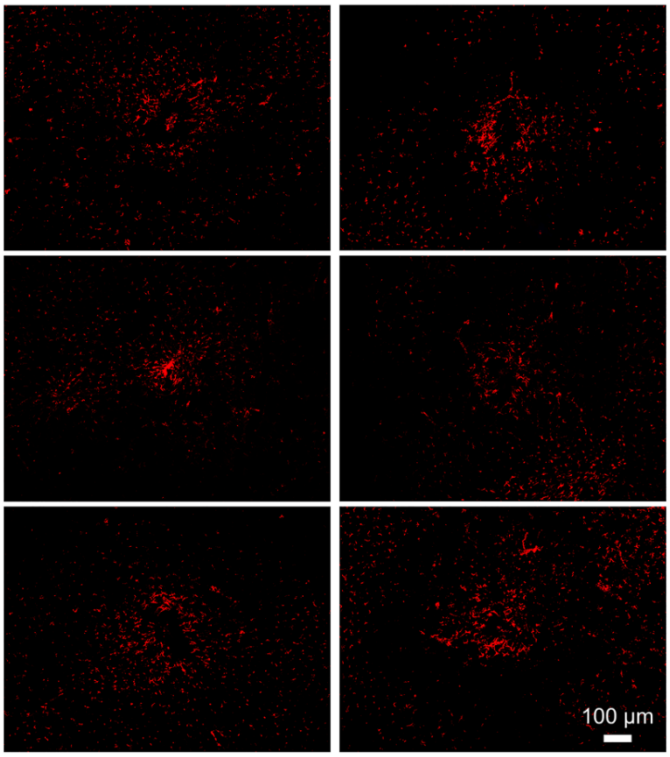

Fig. S15 GFAP immunostaining of octrode arrays after 4 weeks post-implantation.

Representative images were obtained from the subjects in the octrode group (subject number: octrode02-07), respectively. Representative image of subject "octrode01" is shown in Fig. 3b.

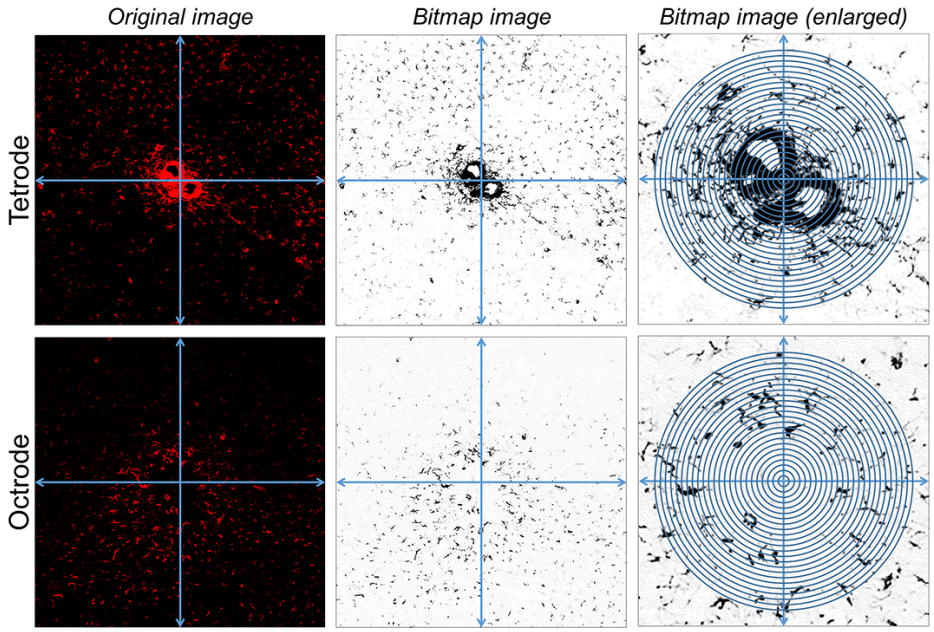

Fig. S16 A schematic diagram of quantitative processing of immunohistochemical data.

The original fluorescent images were converted to bitmap format. Then the immunostaining intensity of GFAP was calculated as a function of distance (stepping distance = 5 μm) to the implant center. The immunostaining intensity of NeuN was analyzed in a similar procedure.

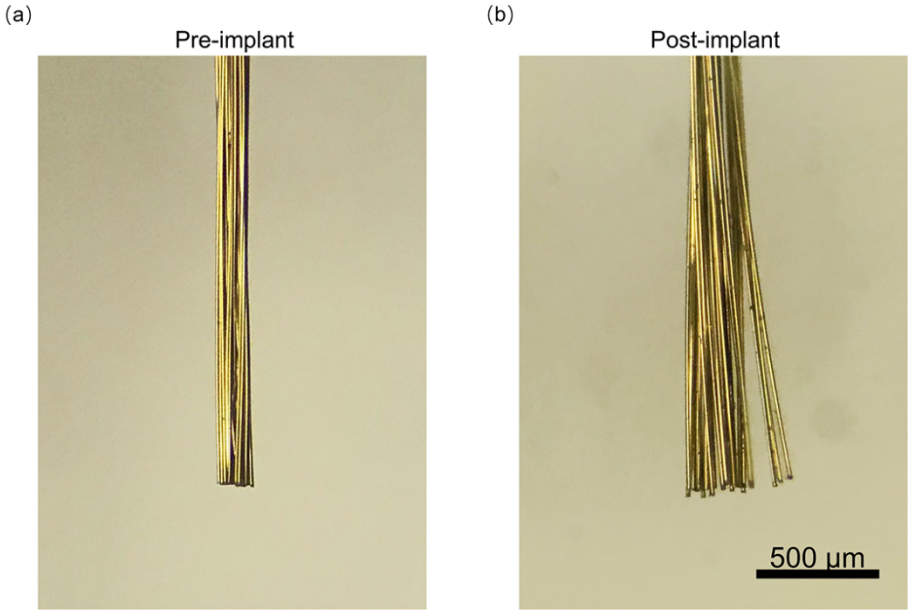

Fig. S17 Representative images of a high-density electrode arrays (32-channel) before and after implantation.

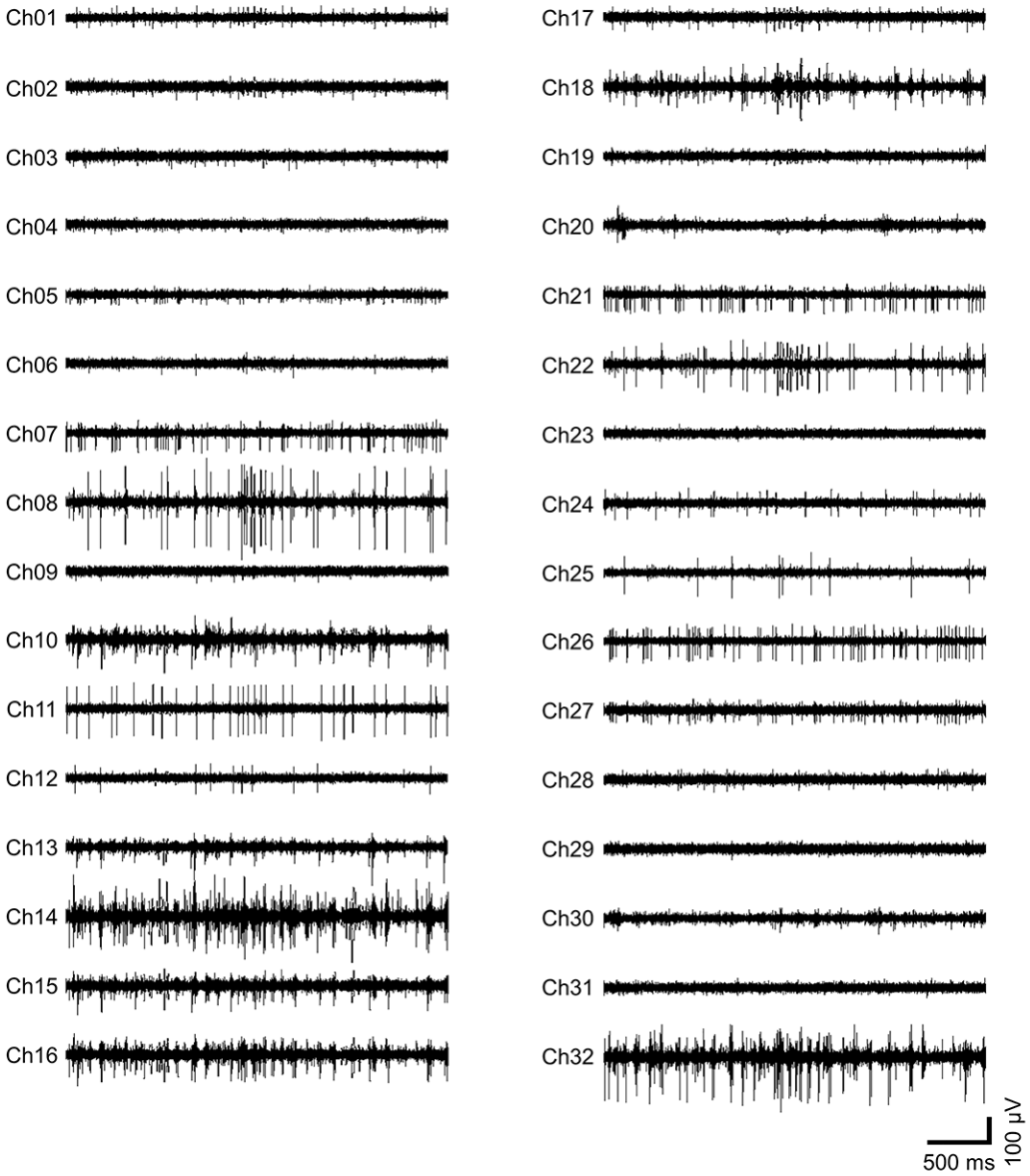

Fig. S18 Representative example of raw spike recordings in hippocampus using a 32-channel electrode array.

The electrode array was fabricated following the similar procedure of octrode arrays. Neuronal activities were detected in more than 90% of the channels during acute electrophysiological recording.